37.3: Limitations of Heat Conductivity in Cryogenic Sensors Due to Surface Roughness

Z. Moktadir[a], M.P. Bruijn[b], R. Wiegerink[a], M. Elwenspoek[a], M. Ridder[b], W.A. Mels[b]

a) MESA+ research institute
University of Twente
P.O. Box 217, 7500 AE Enschede
The Netherlands
email: Z.Moktadir@el.utwente.nl

b) Space Research Organization
Sorbonnelaan 2
3584 CA Utrecht
The Netherlands
email: M.P.Bruijn@sron.nl

Introduction

X-ray astronomy has revealed some of the most exotic and compact parts of the universe. The photometry (counting the number of X-ray photons), imaging (X-ray photons direction measurement) and spectrometry (X-ray photons energy measurement) are techniques that allow astronomers to "see" the surface of pulsars, the close orbit around giant black holes and the blast waves of supernova explosions. To make a highly profitable observation, a high resolution X-ray detection is necessary.

Future X-ray astronomy missions, like NASA's Constellation-X and ESA's XEUS (X-ray Evolving Universe Spectroscopy Mission) require detectors with very challenging specifications. The high energy (0.2 to 10 keV) spectrometer for XEUS aims at: high-energy resolution, $\Delta E_{FWHM} < 2$ eV at 1 keV and $\Delta E_{FWHM} < 5$ eV at 7 keV, high absorption efficiency, > 90% up to 7 keV, a counting rate > 4 kHz, and an imaging capability of typically 32x32 pixels. The type of detector considered most promising is an array of voltage biased superconducting transition edge microcalorimeters, operated at sub-Kelvin temperatures.

Micro-machining technology offers large possibilities for the fabrication of such cryogenic sensors at small scales. Uniformity of response of arrays of these microcalorimeters is critically dependent on the thermal properties of the materials used. Silicon and silicon nitride are materials that are widely used for this purpose. Hence, it is essential to study the thermal properties of these materials at very low temperatures. At milli-Kelvin temperatures, the heat conductivity becomes size dependent (through the mean free path of phonons). In phonon scattering processes at surfaces, the surface roughness plays a fundamental role. In this paper, we will address this topic through a theoretical consideration as well as an experimental approach. As an example, we have calculated the temperature drop in a silicon bar, through which a heat current is driven, as a function of the roughness of its faces.

The paper is organised as follows. The first section is dedicated to the general theory of the size dependent heat conductivity of solids. Next, the problem of the roughness of the surface is addressed, as this is an important effect at sub-Kelvin temperatures. We will also present some results of finite element calculations of the heat transport in a silicon bar. Next, a test structure is discussed that will be used for measurements. Finally, some first results are presented. More results are expected at the time of the conference.

Size-dependent heat conductivity at low temperatures

General idea

In dielectric solids heat is conducted by carriers called phonons. At the macroscopic scale and high temperatures, the transport coefficients (resistance, conductivity, etc.) are characteristic properties of the material and are independent of the shape and the size of the specimen. This is because these quantities are averaged over distances covering many mean free paths and with intervals containing many relaxation times of the carriers.

At very low temperatures, bulk scattering of phonons by impurities, defects, N process and umklapp proces are negligible. In that case the mean free path may become very large and reach the dimensions of the specimen. Thus, phonons will only be scattered by the surfaces of the specimen. Phonons can be scattered specularly (there is no change in the phase of the associated wave) or diffusively (there is a phase randomization). If all phonons hitting the boundaries are diffusively scattered (very rough surface), the mean free path is very close to the diameter of the specimen: this is called the Casimir limit [6]. Then the mean free path is $1.12\sqrt{A}$ for a long square specimen of cross section A, and $2R$ for a long circular specimen of radius R. Since the thermal conductivity κ is proportional to the mean free path, it is given by:

$$\kappa = \frac{1}{3} C^{-} d \qquad (1)$$

0-7803-7454-1/02/$17.00 ©2002 IEEE

where d is the mean free path, C is the heat capacity and $\bar{\upsilon}$ is the Deby average velocity of sound.

On the other hand, it can be shown using the formal transport theory that the scattering process of phonons on the walls of the specimen will be influenced by the surface roughness [1-4]. This phenomenon has been the object of intensive investigations in the case of electronic transport as well [5].

The specularity is the probability that a phonon with a wavelength λ scatters without any change in the phase in its corresponding wave. The mean free path of such a scattering mode will be beyond the dimensions of the specimen. It can be shown that the specularity depends on the surface roughness [4] and is given by:

$$f(\lambda) = \exp(\frac{16\pi^{3}\;{}^{2}}{\lambda^{2}}) \qquad (2)$$

where η is the root mean square roughness of the specimen walls.

At low temperatures, we will use the dominant wavelength approximation, i.e. we consider all phonons to have a single wavelength λ_{dom}, instead of using a distribution of wavelengths. The dominant wavelength is given by:

$$\lambda_{dom} \quad 0.235\frac{h}{K_B}\frac{\bar{\upsilon}}{T} \qquad (3)$$

where K_B and h are the Boltzmann and Planck constants, respectively. For example, at 50 mK the dominant wavelength is λ_{dom} = 1.33 µm, with the value of $\bar{\upsilon} = 5.93 \quad 10^{3} m/s$ [7].

According to [4], the mean free path can be calculated for a rod with a length larger than its diameter, with the formula:

$$l = \frac{1+f}{1-f} l_c \qquad (4)$$

Where l_c is the Casimir limit (the diameter of the specimen). Inserting expression (4) in (2), we have for the heat conductivity:

$$\kappa = \frac{1}{3} C\bar{\upsilon} \frac{1+f}{1-f} l_c \qquad (5)$$

Where the heat capacity is given by: $C \approx 0.66T^{3} JK^{-1}m^{\;3}$. We will use this value for calculations in the next subsection.

Example: finite element calculation of the temperature distribution in a silicon bar

In order to illustrate the above ideas, we present here a model calculation for a part of a sensor, as under study for the XEUS mission. The sensor is an array (5 x 5 prototype) of microcalorimeters. Each pixel consists of a thin film X-ray absorber and thermometer, fabricated on a silicon nitride membrane. In the membrane, slots are etched to tune the heat conductivity to the cold bath. The membranes are attached to silicon support bars (see also fig. 5), which should provide a high thermal conductivity link to the cold bath. Typical width of the bars is 40 µm, the height of the bars is 400 µm (the full wafer thickness). A typical operating temperature is 100 mK. In order to make use of a feedback mechanism the calorimeter is operated well above the bath temperature, which should have a value of about 40 mK. It is important that each pixel sees the same bath temperature. The heat conductivity of a bar must therefore be high enough that under bias conditions (when each pixel dissipates 10 pW) the temperature next to each membrane is within about 10 mK equal. A high thermal conductivity is furthermore important to reduce cross-talk.

For this model we have calculated the temperature distribution in one of the silicon bars. Since the bar is thin, a two-dimensional representation is a good approximation. The heat flow from the membranes is approximated by little cubes of (Si-) material in which a uniform power dissipation is present. We have solved the non linear stationary heat equation:

$$\nabla \cdot (\kappa(T \; \nabla T) = Q \qquad (6)$$

where Q is a constant heat source, and κ is given by (5). This equation will be solved in four sub-domains: three heaters and the silicon bar. We apply the insulation boundary condition $\vec{n}.\nabla T \quad 0$ on all edges except the right edge, which is set at the bath temperature of 40 mK. The result is shown in figure 1 and figure 2. Figure 1 shows the temperature distribution in the silicon bar, in case of a surface roughness η = 40 nm. Figure 2 shows the temperature profile along cross-section AA'(see figure 1), for different values of the surface roughness. We notice that the surface roughness must be in the order of 10 to 20 nm to fulfil the above mentioned requirements on the temperature next to each pixel. In the micro systems field, not all used technologies (growth, etching, etc.) lead to smooth surfaces.

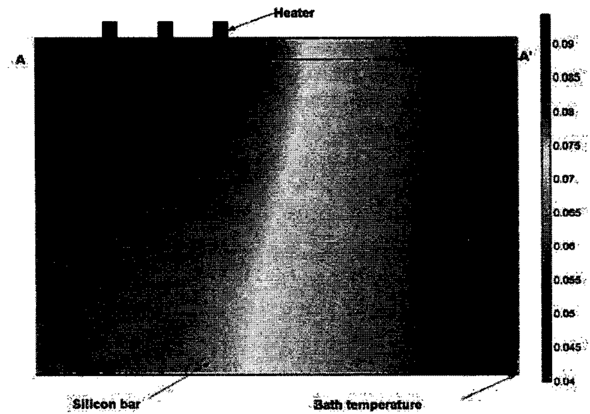

Figure 1. The temperature distribution of silicon Bar subjected to three heaters, for $\eta \quad 40nm$.

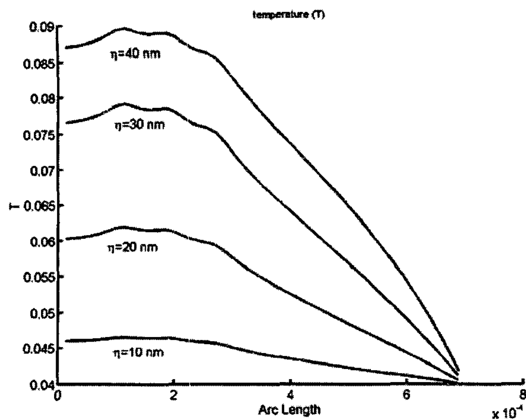

Figure 2. Temperature profile along AA'. The drop in temperature from one edge to the other depends on the surface roughness.

One of the most used technologies is KOH etching. Its simple handling makes it widely popular in micromachining of silicon. However, its anisotropy (every crystallographic orientation has different physical and chemical properties under KOH etching [8]) limits the choice of an appropriate condition that leads to smooth surfaces. The only known crystallographic orientation leading to a very smooth morphology is the {111} orientation [8]. The corresponding value of the rms roughness can reach a few nanometers. This fact seems promising in improving the performance of cryogenic sensors as mentioned in the analysis above. Therefore, a process route based on this method is presently under study. This route is described in the next section.

Experimental design of a support structure for a cryogenic sensor

We have used Si(110) wafers for micromachining of vertical smooth <111> oriented walls. The wafers are coated with low stress silicon nitride on both sides. The first issue to be resolved is the identification of the <111> orientation. The precision of the alignment of the mask is crucial. A misalignment of just 0.05 degrees will already result in an unacceptable under etching of the walls due to the large length of the walls (4 mm). We use a special mask design for this purpose [9]. The process flow is shown in figure 3.

After the lithography of the first mask, the small area in the silicon nitride is opened by the reactive ion etching. The patterned area is then immersed in 25% KOH solution for about 15 minutes at a temperature of $75^{\circ}C$. The resulting geometry after etching will allow the identification of the <111> direction to which the second mask is aligned. The second process step consists of opening areas in the silicon nitride by reactive ion etching. The sides of this area are aligned with the <111> direction as illustrated in figure 4. The sensor structures will be deposited between two consecutive beams on the top of the resulting silicon nitride membrane after KOH etching from the back side. The heat will sink through the silicon beams to the bath linked to the bottom of the wafer. Note that the beams themselves are not connected to the bath, only the bulk silicon is. This structure is used for heat conductivity measurements of both silicon and silicon nitride. This preliminary study is critical before starting any further development.

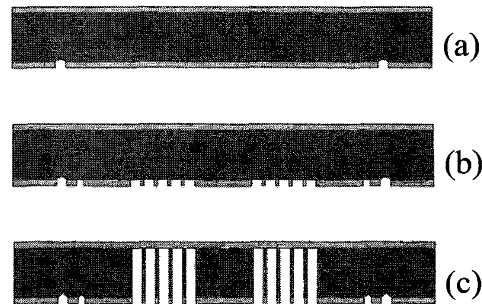

Figure 3. Summary of the process flow of a micromachined support for a cryogenic sensor: a) Start with low stress silicon nitride coated Si, litho/etch back-side nitride and short KOH etch through the first mask to identify the <111> crystal orientation, b) Litho/etch back-side nitride aligned to <111> crystal orientation, c) KOH etch of deep trenches through Si-wafer with smooth <111> side walls..

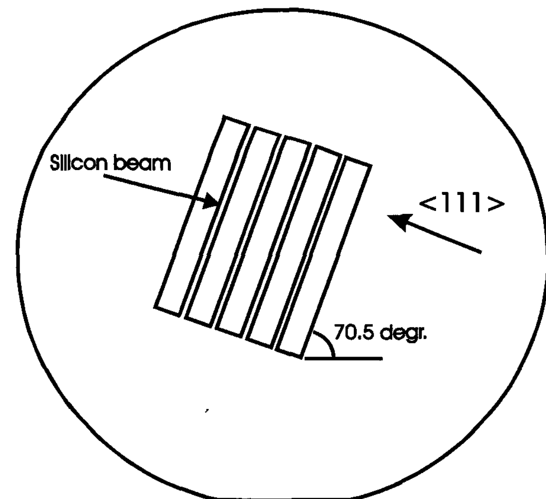

Figure 4. Schematic illustration of the micromachined support for a cryogenic sensor. The silicon beams are bounded by Si(111) smooth walls.

Figure 5 shows the results of the micromachining process. It clearly shows the etched silicon beams and the resulting silicon nitride membranes. The silicon walls are smooth and should result in a good thermal conductivity, as is re-

quired for the sensor array that is considered for the XEUS mission.

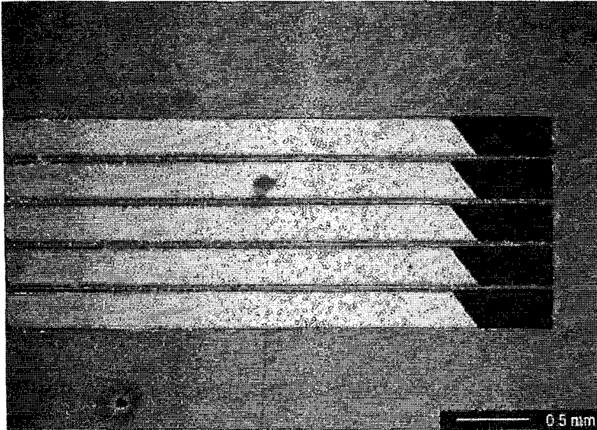

Figure 5. The resulting micromachined structure leading to Si(111) beams.

Experiments

Figure 6 shows a photograph of a complete fabricated test device. On the beams a Cu thin film heater and Ti/Au thermal switches (superconducting transition) were deposited. The bath temperature can be adjusted and for several temperatures the amount of power that has to be applied to the heater in order to switch the thermometers can be measured. The experiments were performed in a dilution refrigerator with a base temperature of 10 mK. Some initial experiments clearly indicate the size dependent effects. However, much more experiments are needed. More results are expected to be available at the time of the conference.

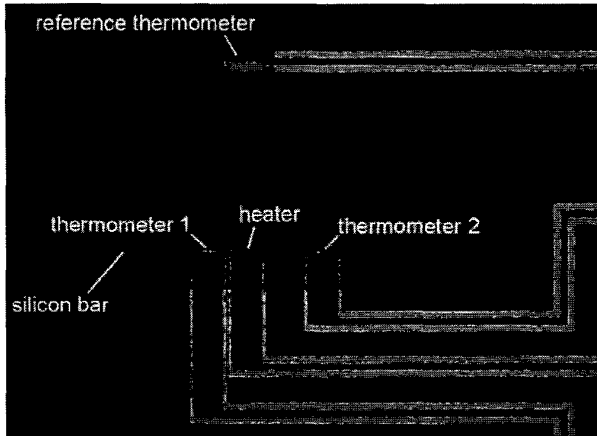

Figure 6. Photograph of the experimental device. The device contains 40 μm wide etched silicon bars with a heater and two thermometer structures on top.

Conclusion and Remarks

In this investigation, we have shown that the performance of a cryogenic sensor should depend significantly on the smoothness of its surfaces. At low temperatures, the heat transport is critical for such sensors. Modeling heat transport at low temperature has always proven uneasy. However, approximate calculations can be made to obtain qualitative results. With the help of the finite element modeling, one can estimate the performance of cryogenic sensor by solving the non-linear heat equation as shown in this paper. We have proposed a relatively easy technology (KOH etching) to obtain smooth structures in silicon. Using KOH etching in Si(110) wafers, leads to smooth Si(111) walls for better heat conductivity and performance of the sensor.

References

[1] R. Berman, E. L. Foster and J. M. Ziman, Proc. Roy. Soc. Lond., A, Vol. 231, 130-144, 1955

[2] R. Berman, F. E. Simon and J. M. Ziman, Proc. Roy. Soc. Lond., A, Vol. 220, 171-183, 1953

[3] P. G. Klemens, Proc. Roy. Soc. Lond, Vol. 208, 108-133, 1951

[4] Ziman, 'Electrons and phonons', Oxford University Press, (1979)

[5] See for example: G. Palasantzas, J. Barnas, Phys. Rev. B, Vol. 56, pp. 7726, 1997

[6] H. B. G. Casimir, Physica 5, 495, (1938)

[7] A. K. McCurdy, H. J. Maris, and C. Elbaum, Phys. Rev. B, 2, 4077, (1970).

[8] K. Sato, M. Shikida, Y. Matsushima, T. Yamashiro, K. Asaumi, Y. Iriye and M. Yamamoto, Sensors and Actuators A 64 (1998), pp. 87-93

[9] Mattias Vangbo and Ylva Backlund, J. Micromech. Microeng. 6, (1996) 279-284.